Table of Contents

Abstract	iv
I. Introduction	1
II. Neutron Converters	5
a) General Considerations	5
b) Gadolinium Converter	8
c) Boron Converter	11
III. Resolution	13
IV. Equipment	17
a) Multiwire Proportional Chamber	17
b) Electronics	17
c) Pressure Vessel and Monitoring	18
d) Calibration Source	20
V. Wire Chamber Performance	23
a) Chamber Amplification	23
b) Efficiency and Cadmium Ratio	24
c) Resolution and Pressure	26
d) Resolution and Bias	26
VI. Summary and Conclusions	33
Appendix A	35
Appendix B	41
References	43
Acknowledgements	45

NOTICE

This report was prepared as an account of work sponsored by the United States Government. Neither the United States nor the United States Department of Energy, nor any of their employees, nor any of their contractors, subcontractors, or their employees, makes any warranty, express or implied, or assumes any legal liability or responsibility for the accuracy, completeness or usefulness of any information, apparatus, product or process disclosed, or represents that its use would not infringe privately owned rights.

Performance of a Pressurized Multiwire Proportional Chamber for Neutron Radiography

Bruce Director
Lawrence Berkeley Laboratory
Department of Nuclear Engineering
University of California, Berkeley
Berkeley, California

ABSTRACT

A study was made of the effect of gas density on resolution and efficiency of a neutron sensitive multiwire proportional chamber. Increasing the density will shorten the reaction products range. A pressure vessel was designed and constructed for 4 atm thereby reducing the range of the reaction products from the neutron converter by a factor of 4, compared to 1 atm. Pressurizing the chamber to 4 atm resulted in a spatial resolution of 1mm under the most favorable operating conditions.

For the type of neutron converters used improving the efficiency is limited to a choice of material. Two different materials were tried, gadolinium and boron, with efficiencies of 6.3 and 2.3%, respectively.

Performance of a Pressurized Multiwire Proportional Chamber for Neutron Radiography

Bruce Director
Lawrence Berkeley Laboratory
Department of Nuclear Engineering
University of California, Berkeley
Berkeley, California

I. Introduction

In the past ten years a new type of particle detector, the multiwire proportional chamber (MWPC) with the ability to detect the position of charged particles has been developed [1]. These chambers have found applications in high energy physics [2], crystallography [3], and biomedical imaging [4]. Among the wire chambers' desirable qualities are high efficiency, good spatial resolution, and very good time resolution.

The basic form of the MWPC is a grid of wires, each acting as an individual proportional counter. By detecting the wire on which the proportional multiplication occurs, a particle's position in the direction perpendicular to the wires can be determined. With a second wire plane perpendicular to the first, and in close proximity, there will be an induced pulse on the second wire plane, so the other coordinate can be found.

For chambers with a relatively few wires it is feasible to attach an amplifier to each wire. For large chambers the cost of individual amplifiers can be considerable. There are a number of schemes to code the position information. A binary coding scheme requires $\log_2 N$ amplifiers. Each wire is assigned a binary number from 1 to N. For each "1" in the binary word the wire would be connected to the corresponding amplifier,i.e. the 41st wire (101001) would be attached to the first, fourth, and sixth amplifier [5].

If all the wires are interconnected by resistors having a small resistance, the pulse will be attenuated by an amount proportional to the resistance encountered by the pulse in traveling down the resistor string, i.e. the distance. The pulse heights from different pulses are not

constant. To obtain position information the pulse height from both ends of the resistor string has to be compared [5].

By adding a third wire plane there are some simple and easy read-out methods. The middle plane (anode) acts as the proportional counter. The outer two planes (cathodes) are oriented perpendicular to each other. A pulse on the anode will induce a pulse on each cathode plane. In the charge division method, each cathode plane is wound with resistive wire, as one continous wire. The ratio of the charge collected at one end of the wire to the total charge gives the relative position along the wire.

Each wire in the grid has some self-inductance so it acts as a delay line. By measuring the delay of the signal from one end of the wire plane relative to the other the particles' position can be determined. Perez-Mendez [6] extended this idea by developing inexpensive delay lines. In this method the signals on the cathode wires are coupled to the delay line. With a prompt signal derived from the anode plane an oscillator and counter can be started. The delayed cathode signal provides the stop signal. The number of counts is proportional to the distance. An alternate method, used in this work, is to use a time-to-amplitude converter (TAC), giving an output voltage proportional to the distance along the delay line. Each of these is easily digitized for use with computerized image enhancement.

Charpak [7] has shown, for multiwire proportional chambers, that the equipotential lines near an anode wire are circular, as in a single cylindrical proportional counter. Since the electric fields in the two detectors are the same, the theoretical development behind the proportional counter is applicable to the wire chamber. Specifically, the pulse formation in a wire chamber will follow the same time development as in the proportional chamber.

Because the wire chamber responds only to charged particles it is necessary to convert the neutron to a charged particle to be detected. This problem is encountered in all forms of neutron detection and there are a few well used materials employed as neutron converters. K. Valentine [8], the first to use wire chambers for neutron imaging, used a solid boron converter. As will be shown later one disadvantage of solid converters is their rather low efficiency. In an

attempt to improve this, Valentine tried a combination of front and back converters and increased the efficiency to 3.76% with a resolution of 2.5 mm.

The most commonly used material for neutron conversion is boron triflouride gas. R. Allemande [9] has built two wire chambers using BF_3 with efficiencies of 40 and 70%. They found a resolution of 2.6 mm, which is slightly greater than the particle track length of 2.5 mm. One disadvantage of BF_3 is that it is not a very satisfactory filling gas. It is a very reactive gas and must be handled carefully. It breaks down in the presence of moisture and the detection efficiency is a function of temperature. With a solid converter the filling gas can be optimized for the particular application.

Another gas that has come into recent use is ^3He, which undergoes the reaction $^3He(n,p)^3H+764keV$. J. Alberi [10] has used this gas in a two dimensional wire chamber for use with small angle neutron scattering. To decrease the neutron mean free path and to shorten the particle range a filling gas of 3 atm. ^3He and 6 atm. Ar was used. The chamber thickness was large enough such that the detection efficiency was almost 100 %. However, the rather long total track length resulted in a resolution of 3.1 mm.

The last use of a neutron sensitive wire chamber that will be mentioned was for the detection of high energy (15 to 20 GeV/c) neutrons produced in the decay of subatomic particles. M. Atac [11] built a detector that consisted of 5 wire chambers with each chamber having its own steel plate neutron converter. Interaction in the converters produced a shower of particles. By fitting the data in all five chambers, there was an overall resolution of 7 mm.

These examples indicate a relationship between resolution and particle range, i.e the shorter the particle range the better the resolution. The efficiencies of wire chambers using gas converters is a function of the chamber thickness so that 100% efficiency can be obtained by making the chamber thick enough. Efficiency with solid converters are determined by the nuclear properties of the material and so in general are limited to a choice of material.

The two (solid) converters used in this work were gadolinium and enriched boron. Gd is the preferred converter for photographic radiography because the 70 keV conversion electron

emitted has a range of only 50 μm in photographic emulsion. Gd has the largest thermal neutron cross section of any naturally occurring element; thus is should provide increased efficiency compared to boron. The range in argon of the conversion electron is 4 cm. To reduce this and to investigate the relation between particle range and spatial resolution, the chamber was placed in a pressure vessel that can be pressurized to 4 atm. This reduces the particle range by a factor of 4. The range of the conversion electron at 4 atm. is approximately equal to that of the α particle from ^{10}B at 1 atm. So a 4 atm. MWPC using P-10 gas (90% argon and 10% methane) in conjunction with a ^{10}B converter was expected to yield excellent resolution. In another attempt to improve resolution the effects of biasing the cathodes was investigated.

II. Neutron Converters

a) General Considerations

Any element can be used as a neutron converter since all absorb neutrons to some degree. But to obtain reasonable efficiency the material should have a large absorption cross-section. Another criterion is that the reaction products should have a small range in the chamber. Fig. 1 is a graph of the range of α's, electron's and γ's in argon. It can be seen that the gamma ray ranges are an order of magnitude larger than the charged particle ranges, so those materials that undergo (n,γ) reactions are unsuitable.

Not all reaction products reach the surface of the converter. That fraction that does reach the surface, the maximum efficiency for the converter, is given by

$$\tfrac{1}{2}\left[1-\frac{\lambda}{R}+\frac{\lambda}{R}e^{-R/\lambda}\right]^{*} \tag{1}$$

with λ the neutron mean free path in the converter and R the range of the particle in the converter. A plot of this function is shown in fig. 2. The curve asymptotically approaches 0.5 as a maximum efficiency, as the range, expressed in terms of the neutron mean free path R/λ, increases. Reaction products are emitted isotropically following thermal neutron capture and even if they had an infinite range, one-half would still be emitted in the "wrong" direction, to the side opposite the wire chamber.

---

* The fraction of absorbed neutrons between x and dx (x measured perpendicular to the surface of the converter) is

$$P(x)\,dx = \Sigma_a e^{-\Sigma_a x}dx$$

where Σ_a is the absorption cross section. To reach the surface, the particle has to be emitted within an angle θ given by $\cos\theta = \frac{x}{R}$. With $f(\cos\theta)$ the angular distribution of reaction products,

$$\text{fraction reaching the surface} = \tfrac{1}{2}\int_0^R \Sigma_a e^{-\Sigma_a x}\int_1^{\frac{x}{R}} f(\cos\theta)\,d(\cos\theta)\,dx \tag{A}$$

For particles emitted isotropically $f(\cos\theta)=1$. Integrating eq. A yields equation (1).

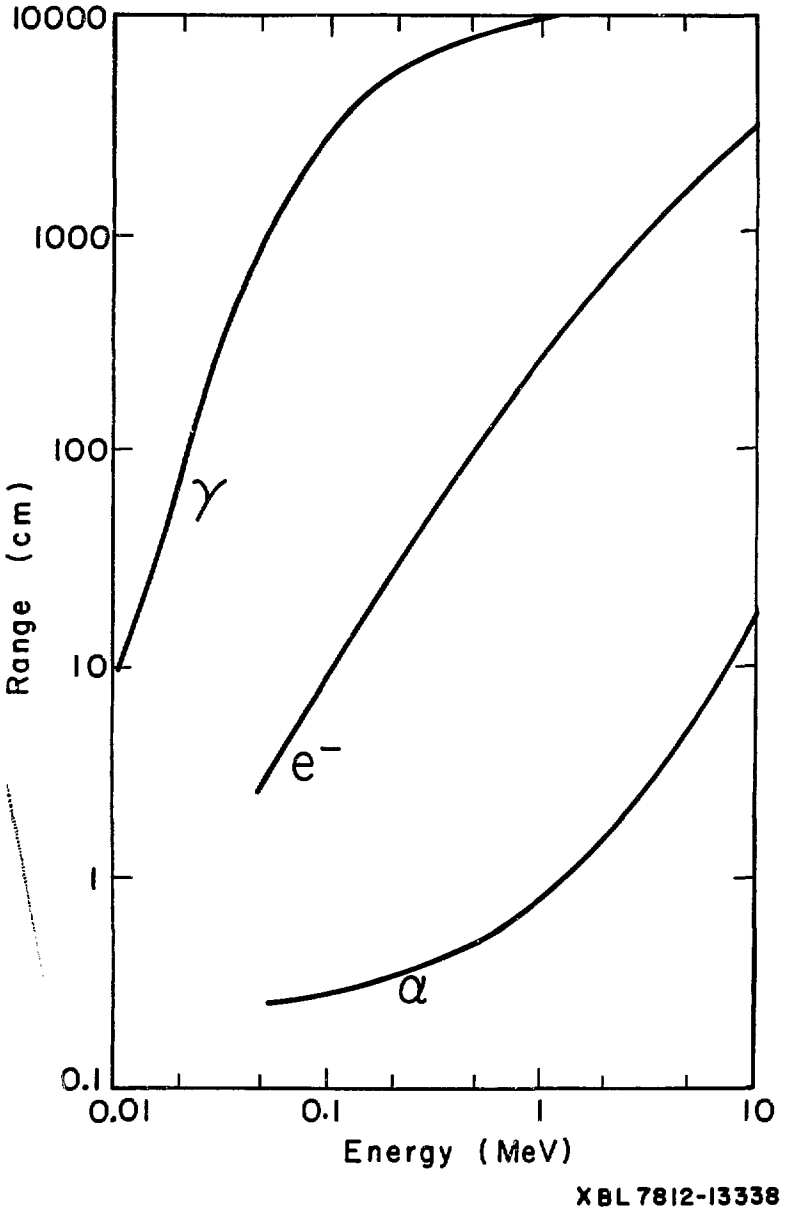

Fig. 1. Range of alpha's, electrons, and gamma ray's in argon at 1 atmosphere. The gamma ray "range" is one mean free path.

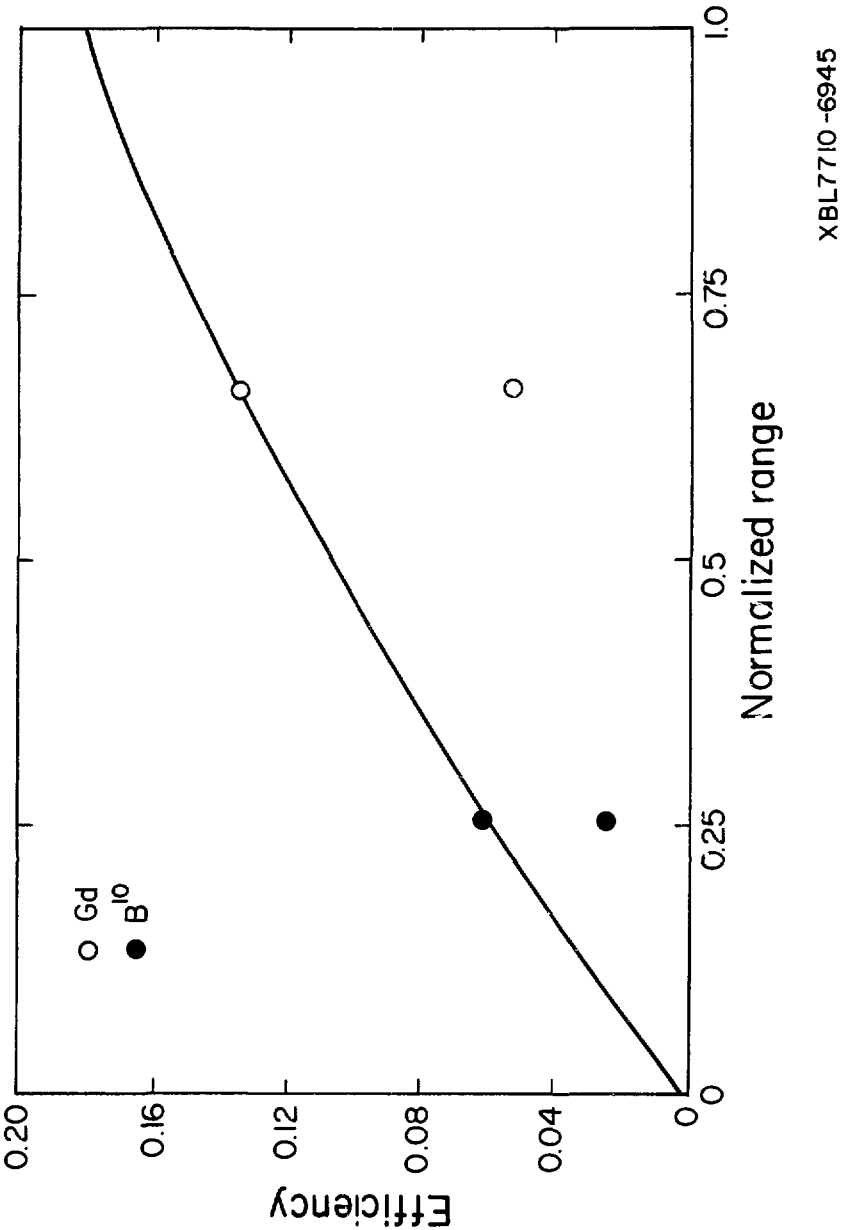

Fig. 2. Maximum efficiency, $\frac{1}{2}[1-\frac{\lambda}{R}+\frac{\lambda}{R}e^{-R/\lambda}]$, as a function of the normalized range, R/λ. The points off the curve are the measured values. The points on the curve are the maximum efficiencies for ^{10}B and Gd.

Solid converters have an inherent focussing effect that is not present in gas converters. Reaction products from a depth x in the converter have to be emitted within a critical angle, equal to $\cos^{-1}\frac{x}{R}$, in order to reach the surface. As the depth of interacton increases, the reaction products are emitted in a narrower and narrower cone about the normal. The dispersion about the normal is reduced, leading to improved resolution, but reduced efficiency. For example, as R/λ goes from .25 to .5 the efficiency will increase by 84% (to a value of .1 which is low compared to gas filled wire chambers) but the resolution will be decreased by 25%.

b) Gadolinium Converter

Of the two converters used gadolinium has the larger R/λ and a maximum efficiency of 15.3%. The decay scheme for gadolinium is shown in fig.3a. There are two isotopes, ^{155}Gd and ^{157}Gd with cross sections of 58,000 b and 254,000 b. After neutron capture the most probable decay is to the first excited state of ^{158}Gd From the first excited state there are two decay possibilities, either gamma emission or internal conversion. The gamma ray has an energy of 79 keV and the conversion electron has an energy of 79 keV minus the binding energy of the shell it was emitted from. For the K and L shell electrons the resultant energies are 30 and 70 keV, respectively. The internal conversion coefficients are α_K=2.14 and α_L=3.34 [12]. So 84% of all transitions from the first excited state result in conversion electrons. The ratio of 70 keV electrons to 30 keV electrons is 1.56/1.

The conversion electrons leave the converter at some angle and with some residual energy. Fig. 4a is a plot of the locus of endpoints for 70 keV electrons in the detector. The distance from the surface of the converter to a distance equal to the range of the electron (in gadolinium) was divided into 25 equal intervals. At 1° steps from 0° to the maximum emission angle, the residual energy of the electron in the converter, and the range in the gas were calculated. Since the particle is well localized in the converter it was assumed that the electron emerged into the gas from the point where the neutron entered the converter. The electron range and energy were calculated using the Katz and Penfold [13] empirical formula, with a

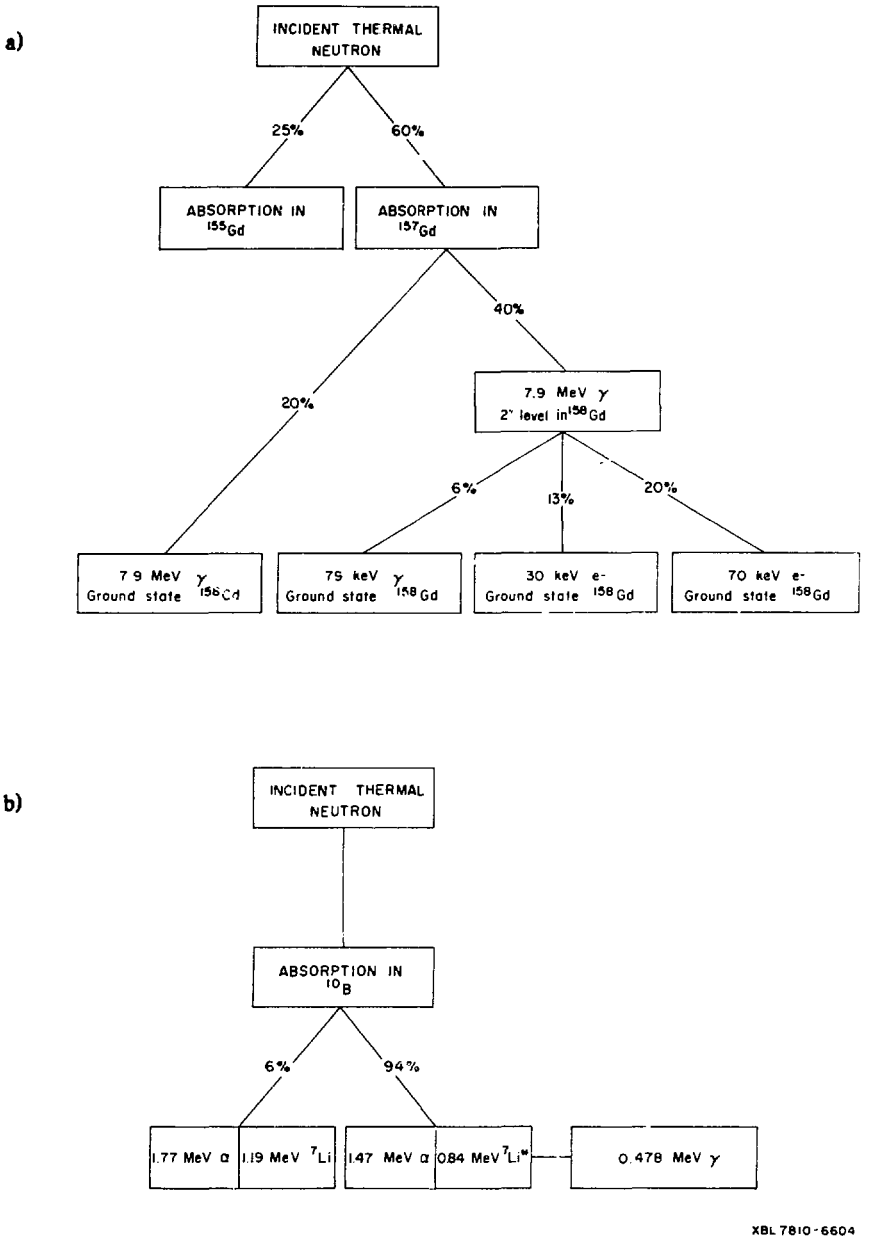

Fig. 3. Decay scheme for a) Gd and b) ^{10}B. The numbers in each channel are the fraction of incident neutrons in the given channel.

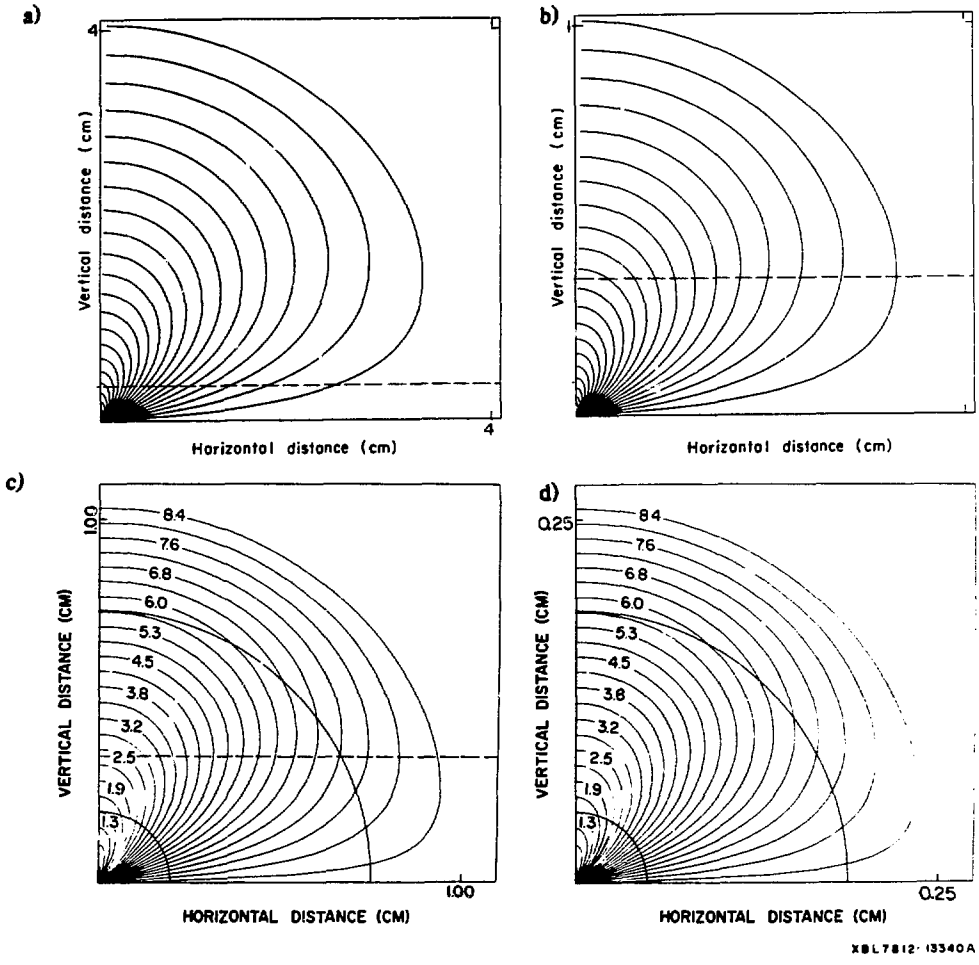

Fig. 4 Plot of the locus of endpoints of the reaction products emerging from different depths in the converter for a) Gd converter at 1 atm. b) Gd converter at 4 atm. c) ^{10}B converter at 1 atm. d) ^{10}B converter at 4 atm. The horizontal lines indicate the position of the anode. There is no line on d because the anode is located at a distance of 0.3 cm and is off scale. Curves c and d were taken from reference 8.

correction for different atomic number [14].

The measured spectrum of conversion electrons from Gd is shown in fig. 5. There are no prominent peaks chaaracterizing the monoenergetic 30 and 70 keV electrons. This absence of observed structure is not surprising since the electrons lose a significant fraction of their energy in passing through the Gd and those with large energies will have a range larger than the chamber thickness so will not deposit their full energy. From fig. 4, even at 4 atm, the electrons possess enough energy to pass through the active region.

The Gd converter was made by epoxying a 3 mil natural Gd foil on the face of an aluminum frame.

c) Boron Converter

For the boron converter the reaction is $^{10}B(n,\alpha)^{7}Li$ with a Q value of 2.3 MeV. The α particle has an energy of 1.5 MeV and the ^{7}Li an energy of 0.8 MeV. See ref. 8 for the spectrum of α's from the boron converter. Fig. 4c is a plot of the locus of particles from the boron converter. The maximum distance from the point of interaction is about 1 cm compared to 3.2 cm for the electrons.

Strips of 1" wide double sided pressure sensitive tape were attached to one aluminum frame and 92% enriched ^{10}B powder was dusted into it to make the boron converter.

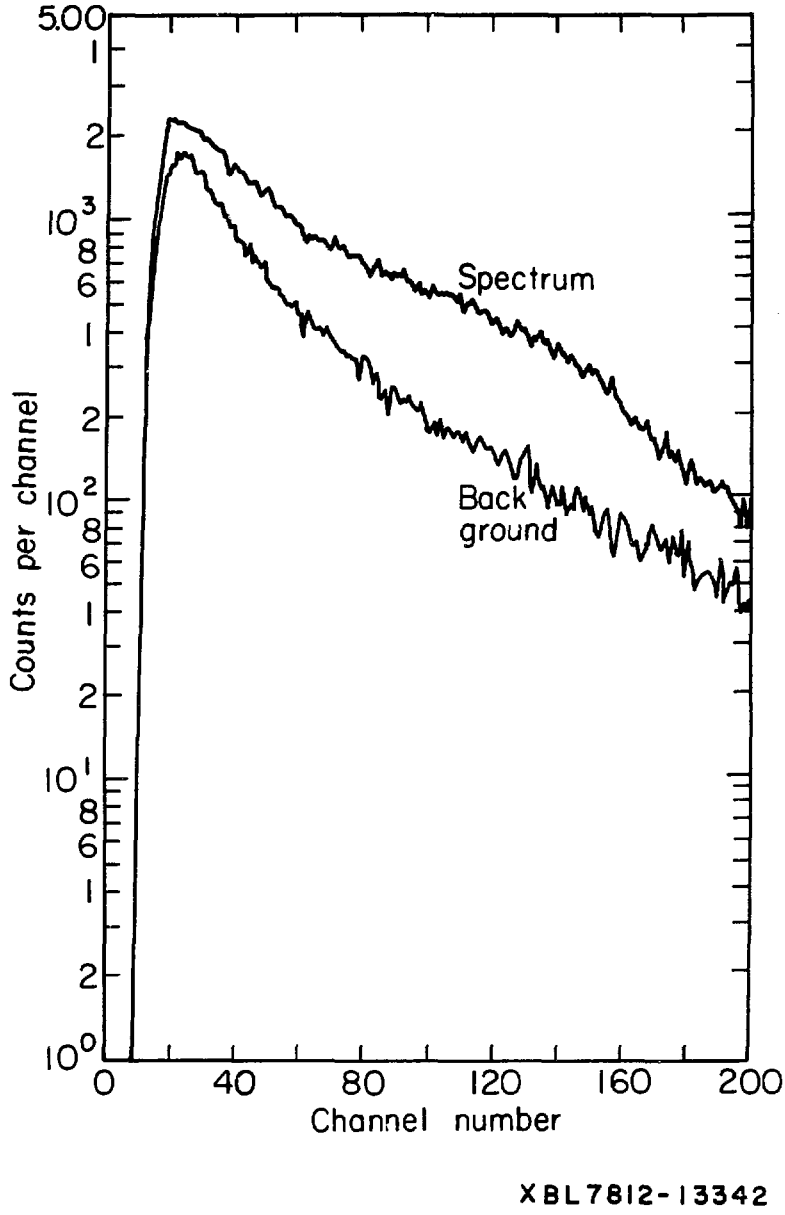

Fig. 5. Conversion electron spectrum from Gd. The background was taken with a Cd sheet covering the chamber, so the background consists of gamma rays plus epithermal and fast neutrons.

III. Resolution

There are a number of ways to measure resolution, among them standard test patterns such as the System Image Quality Indicator [15], ASTM Image Quality Indicator [16], Visual Reading Image Quality Indicator [17], and resolving power tests (a series of straight lines or circles with variable spacing). All of these are semi-quantitative in that they require visually determining which image or line is resolved. A quantitative method of measuring resolution is to use the modulation transfer function (MTF).

The two dimensional projection of any object can be decomposed into an infinite series of spatial frequencies, in the same way that a function in the time domain can be decomposed into its component frequencies (Fourier analysis). In passing through a system such as the detector the amplitude and phase of each spatial frequency of the object is changed. The function that describes these changes is called the optical transfer function (OTF). In general the OTF is a complex function. Once the OTF is known the effect of the detector is completely described.

$$IMAGE(\omega) = OTF(\omega) \times OBJECT(\omega) \tag{2}$$

where IMAGE(ω) and OBJECT(ω) are the transforms of the image and object. Eq. 2 is the basis for measuring the OTF. Rearranging gives: $\mathrm{OTF}(\omega) = \frac{\mathrm{IMAGE}(\omega)}{\mathrm{OBJECT}(\omega)}$. The Fourier transform can always be found (with enough computer time). The spatial frequency components that comprise the image are infinite in extent. To measure these the detector should be infinitely large. Using a detector of finite size is equivalent to truncating the output of an infinite detector. To include the effects of truncation, eq. 2 should be multiplied by the Fourier transform of a step function, $\frac{\sin \omega a}{\omega a}$* (2a is the length of the step).

* All Fourier transforms are derived using the following transform pair:

$$F(\omega) = \int_{-\infty}^{\infty} f(x) e^{-i\omega x} dx$$

$$f(x) = \frac{1}{2\pi} \int_{-\infty}^{\infty} F(\omega) e^{i\omega x} d\omega$$

The output of the detector, whether it is digital (counts in a memory) or analog (dots on a photograph) is a distribution of intensity. The phase is not measured. The modulation transfer function is the normalized absolute value (intensity) of the optical transfer function. The normalization is obtained by dividing by the steady state response, which normalizes the MTF to values between 0 and 1.

$$MTF(\omega) = \left| \frac{OTF(\omega)}{OTF(0)} \right| \tag{3}$$

MTF curves have the same basic shape, starting at a contrast equal to one at zero frequency and monotonically decreasing to zero at some high frequency (cutoff frequency).

It has been suggested that MTF's can be fitted to a curve of the form $e^{-(\frac{\omega}{\omega_c})^n}$ [18]. For reasonable MTF's the exponent will be a number between 1 and 2. The quantity ω_c characterizes the slope of the curve and is known as the "critical frequency". When the frequency equals the critical frequency the contrast is .369 independent of the exponent, so the critical frequency can be used to compare different MTF's. However the most common way of measuring resolution is the resolving power test, and what would be useful is to derive a single number from the MTF curve that can be used to compare with the single number that is reported as the resolution when the resolving power test is used.

Consider an infinite bar pattern with a period p. If the input is expanded in a Fourier series the fundamental frequency will be $\frac{1}{p}$ and the series is

$$\sum_{n=1}^{n=\infty} \frac{\sin nx/p}{n/p} \qquad n=1,3,5,\cdots \tag{4}$$

The effect of the detector on the above Fourier series is to multiply the coefficients by the MTF contrast at the frequency $\frac{n}{p}$. For $\frac{n}{p}$ greater than the MTF cutoff frequency all the coefficients will be multiplied by zero. The output, expressed as a Fourier series, will have a finite number of terms, with the same frequencies as the input series and the coefficients related to the

coefficients of the input series by the MTF. As the period of the bar pattern is decreased (and the fundamental frequency increases) the number of terms in the output series will decrease until the fundamental frequency equals the cutoff frequency, at which point there will be no output. It is this point that is measured by the resolving power test and it corresponds to the MTF cutoff frequency [19].

A delta function has a Fourier transform of unity, that is it has all frequencies present with equal amplitude. Using a delta function as the object, the OTF is simply the Fourier transform of the image. In practice a delta function is approximated by a narrow slit, the width of the slit being small compared to the relevant dimensions of the detector. Experimentally, a slit has a finite width, which modifies the transform of the image to $\frac{\sin \omega a}{\omega a}$ (with a slit width of 2a). This fact and the ease of calculating the MTF probably led to its being the usual way of finding the MTF. The size of a typical slit for use in this chamber is 1 mm with the chamber dimensions being 25 cm by 25 cm. Measuring the resolution this way measures the response in a small , limited area of the detector. It would be much more desirable to measure the response over the whole chamber. To do this a series of bar patterns were constructed from cadmium strips. The patterns were large enough to cover the entire active area of the chamber. The Fourier series expansion , eq. 4, gives only the odd multiples of the fundamental frequency. To cover a sufficient range two patterns were used. The MTF is then the average response over the whole chamber. In practice the two repetitions on each end were discarded because they never ended on a full cycle. To be totally accurate an infinite number of cycles in the bar pattern is needed because truncating gives other frequency components as well as changing the amplitude. The Fourier transform of a truncated square wave with N bars is $\frac{\sin 2N\omega a}{2\pi\omega \cos \omega a}$. If a sufficient number of cycles are used (seven or more) then the difference between the truncated and infinite series is negligible [20]. The MTF from a bar pattern is compared to one obtained from a slit in fig. 6.

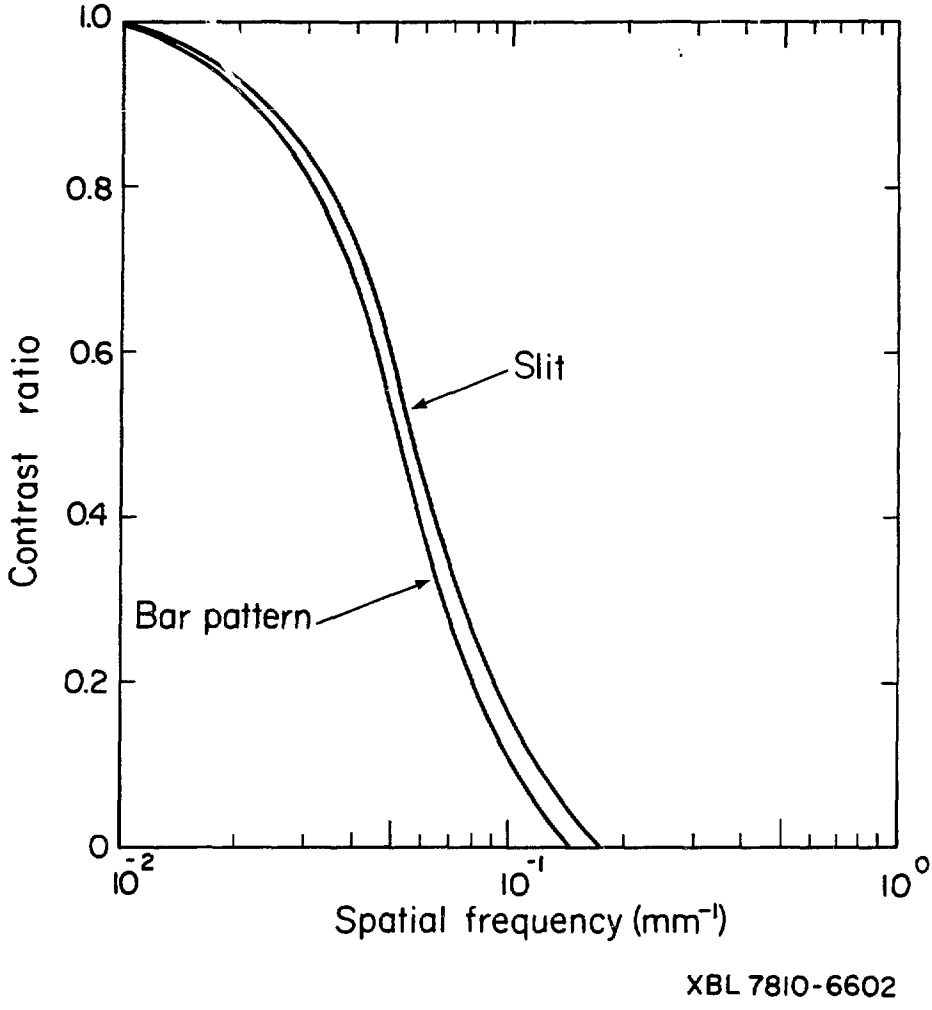

Fig. 6. *Comparison of the modulation transfer function (MTF) from a slit image and bar pattern image.* The Gd converter at 3 atm was used. There is a 7% difference in the two.

IV. Equipment

a) Multiwire Proportional Chamber

The wire chamber used is essentially that described by Valentine [8]. It consists of three wire planes wound on fiberglass frames. The cathodes, spaced 6 mm apart, are wound from 37 μm gold plated tungsten wire. One side of each cathode plane is capacitively coupled to an electromagnetic delay line, with a delay of 6.8 ns/mm. On the other side each wire is tied through a 220 kΩ resistor to a common bus. Under the simplest operating conditions the bus is grounded. However, it is also possible to apply a bias voltage to the bus. The anode is situated halfway between the cathodes. Enough high voltage is placed on the anode so the chamber is operating in the proportional region.

The front face of the chamber proper is covered by a thin aluminum foil to keep photo-and-compton electrons produced in the outer pressure vessel volume from drifting into the active region.

Converter plates can be attached to either the front or back of the wire chamber, and in either case are held in place 0.5 mm from the cathode. The converters used in this work were used exclusively as back converters.

b) Electronics

A charged particle in the chamber results in an anode pulse and two induced cathode pulses. The three pulses are processed through charge sensitive preamplifiers and timing discriminators. The anode signal provides the start signal for two time-to-amplitude converters (TAC's). The signals from the cathodes provide the stop signals. The voltage from the TAC is proportional to the delay, i.e. to the distance the signal traveled along the delay lines. When the output of both TAC's have stabilized, a validate pulse is generated. With the TAC outputs going to the X and Y inputs of an oscilloscope, the validate pulse is used as an intensify signal. A camera placed over the scope face will record the image as a pattern of dots. With a TAC

output going to a multichannel analyzer the validate is used as a coincidence signal. A block diagram of the wire chamber and electronics is shown in fig. 7.

c) Pressure Vessel and Monitoring

When it was decided to pressurize the chamber, it was clear that the wire chamber, originally constructed as a gas flow type, would not hold the desired pressure (4 atm.). The simplest idea seemed to be to build a pressure vessel large enough to hold the wire chamber. Even though the maximum pressure is rather low, the front face would have a large surface area such that the stress on it would be very large. The formula for the maximum stress on a square plate, which is at the center of the plate with length a , thickness t, and under a pressure q is [21]

$$\sigma = \frac{\beta q a^2}{t^2} \tag{5}$$

β is a geometry factor equal to .278. For a 20"x20"x1/2" plate the maximum stress is 27,000 lbs/sq.in. The yield point, the stress that will cause a permanent set of .2%, is 32,000 lbs/sq.in. for standard type 6061 aluminum [21]. For an increased safety margin a high strength aluminum (type 7075) with a yield point of 73,000 lbs/sq.in. was used for the top and bottom plates. The sides of the pressure vessel were made from 3" aluminum channel. Both plates are held to the sides by forty 3/8" bolts. The average stress on each screw is approximately 4000 lbs/sq.in., which should be no problem since each screw is rated at 72,000 lbs/sq.in. A 1/8" thick neoprene gasket seals the plates to the sides.

A thick pressure vessel window will scatter incident neutrons thereby reducing efficiency as well as degrading image quality. At a thickness of 1/2" 10% of the neutrons incident on the front face will be scattered, so to reduce the scattering, an area over the active area of the chamber was milled out to a depth of 1/4".

Decreasing the plate thickness and having sharp edges around the milled out area will increase the stress. Two cases present themselves in which the calculated stress on the milled

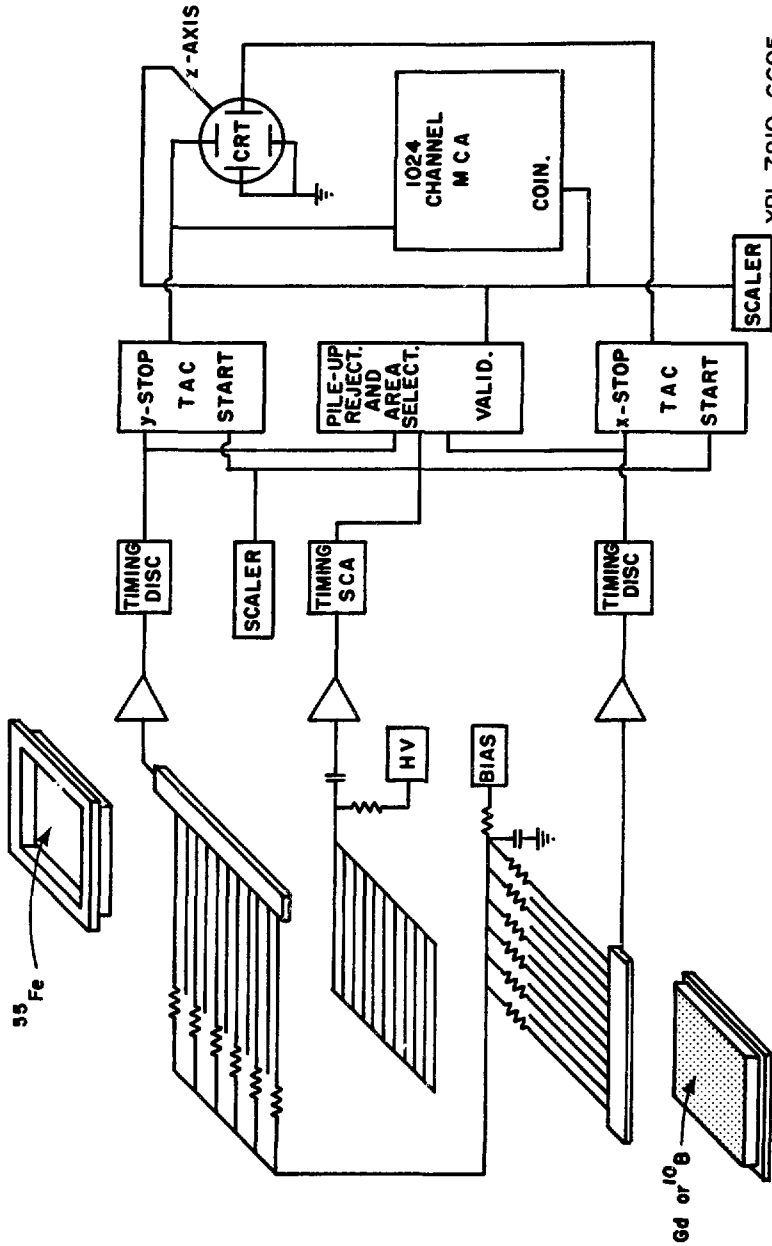

Fig. 7. Schematic diagram of the wire chamber and electronics.

out plate should bracket the actual stress on the plate. First, if the plate were 1/4" thick and 20" on a side, the maximum stress would be 107,000 lbs/sq.in. The other case is the one presented earlier, a 20"x20"x1/2" plate , in which case the maximum stress would be 27,000 lbs/sq.in. To see if the vessel would be safe to use it was hydrostatically tested at 70 psi. There were a few small leaks. After tightening the bolts around the leaking area the vessel held pressure for 24 hours. Fig. 8 is a drawing of the pressure vessel.

To obtain reproducible results it was found necessary to monitor carefully the pressure. A pressure transducer is incorporated in the gas filling system. The pressure transducer is a differential type, good in the range ± 25 psi. With a 3½ digit digital voltmeter to measure the voltage, the transducer is accurate to .5%. See Appendix B for details.

d) Calibration Source

An ^{55}Fe source was deposited in one corner of the aluminum foil covering the chamber. The ^{55}Fe has two purposes. If the source is visible in the oscilloscope display (fig. 9a) the overall system is operating properly. When the pressure is changed the high voltage has to be increased to keep the chamber operating in the proportional mode. To be able to compare measurements made at different pressures the overall gain should be kept constant. The ^{55}Fe is used for this gain normalization.

The source was prepared from a commercial 1 mCi ^{55}Fe solution (120 microliters of $FeCl_2$ in .5N HCL.) Starting with 25 μl of the solution, two serial dilutions were performed, first by a factor of 10, then by a factor of 100. Four drops of this solution, approximately 2 μCi were evaporated in one corner of the foil. With the rest of the foil masked the source was sealed by spraying it with a clear acrylic. The ^{55}Fe spectrum is shown in fig. 9b. The full width at half maximum is 18%.

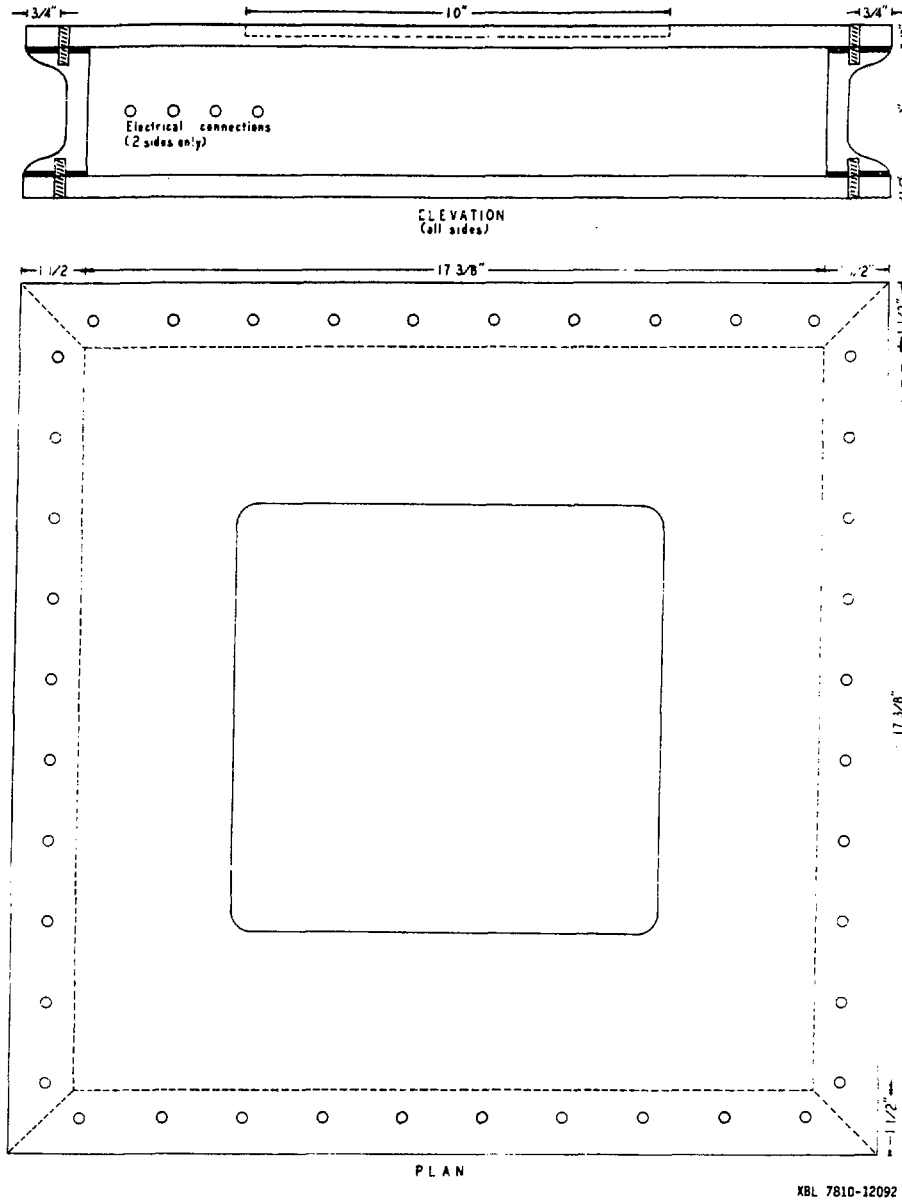

Fig. 8. Elevation and plan view of the pressure vessel.

a)

b)

XBB 780-15270

Fig. 9. a) ^{55}Fe source in the analog display. The three dots in the corners are fiducial marks indicating the extent of the active area of the chamber. The fourth (in the lower left) is obscured by the oscilloscope beam. b) ^{55}Fe spectrum taken at 1 atm. The low energy peak is the 3 keV escape peak.

V. Wire Chamber Performance

a) Chamber Amplification

The wire chamber is operated as a proportional chamber; i.e. the amount of charge detected is equal to the charge deposited by the conversion particle times some constant G (the gain). The number of ion pairs formed by the primary particle is very large and is over a small distance, so the process can be treated statistically i.e.. the number of ion pairs created in a small distance dr is

$$dN = \alpha N\, dr \tag{6}$$

The constant α is called the first Townsend ionization coefficient (measured in ion pairs per mm). Integrating eq. 6 yields

$$\frac{N}{N_0} = G = e^{\alpha r} \tag{7}$$

If the electric field is not constant then α is not constant. At a certain distance from the anode wire, r_0, a primary electron will acquire enough energy between collisions to cause ionization to take place The gas amplification is now given by

$$\ln G = \int_a^{r_0} \alpha dr \tag{8}$$

It has been shown that α/p (p is the pressure) is a function of S (=E/p, E the electric field). Substituting S(r)=V/(pr ln(b/a)) into the above equation yields

$$\frac{\ln G}{paS(a)} = \int_{S(r_0)}^{S(a)} \frac{\alpha(S)dS}{pS^2} \tag{9}$$

For the range of S used with this detector the ionization coefficient is almost proportional to S and can be approximated by $\frac{\alpha}{p}$=CS [22]. Performing the integration with this function gives

$$\frac{\ln G}{paS(a)} = Cln\frac{S(a)}{S(0)} \tag{10}$$

A least squares fit to eq.10 was performed. The results are shown in fig.10. The maximum deviation from the measured voltages is 5%. Although the voltage-pressure relationship is very nonlinear, in the range of operating conditions for this particular detector a straight line is a very good approximation.

b) Efficiency and Cadmium Ratio

The measurements of efficency and resolution were done by placing the wire chamber in a beam port of the Berkeley Research Reactor. A collimator had been placed in the beam tube to provide a point source of neutrons [8]. The cadmium ratio at the position of the wire chamber was measured and had a value of 6.

Efficiency in this case means the ratio of the detected thermal neutron flux to the thermal flux as measured by the gold-foil coincidence method, in the beam port. The detected thermal neutron flux is found by measuring the countrate, over a specific area with and without a cadmium sheet covering the area. The efficiency and cadmium ratio are calculated as follows:

$$\text{efficiency} = \frac{\text{flux(uncovered)} - \text{flux(covered)}}{\text{flux(gold foil)}} \tag{11}$$

$$\text{cadmium ratio} = \frac{\text{flux(uncovered)}}{\text{flux(covered)}} \tag{12}$$

The flux in the above equations is the detected flux.

For the Gd and ^{10}B converters the measured efficiencies were 6.3% and 2.3%, respectively. The efficiencies were unaffected by pressure. The ratio of calculated to measured values is the same for both converters, about 2.7. The gold foil measurement was done at a power of 1 megawatt. The flux used in the denominator of eq.11 was determined by scaling down the ratio of the power at which the measurement was made (100 watts for Gd and 1000 watts for ^{10}B) to 1 MW. But temperature effects and flux depression with the control rods inserted may

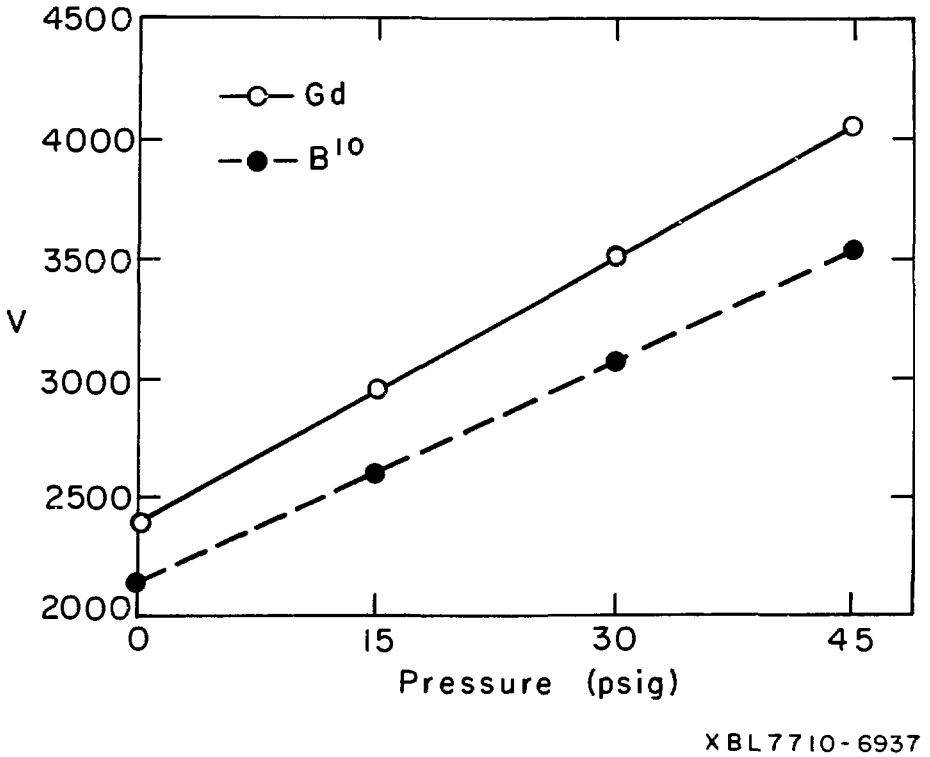

Fig. 10. Operating voltage of the wire chamber vs. pressure for constant gain.

have made this linear scaling somewhat inaccurate.

The Cd ratio for Gd decreased from 8 to 2 as the pressure was changed from 1 to 4 atm. The decrease with pressure is due presumably both to the increase in the macroscopic cross section for γ rays and to the increase in the effective track length, and therefore signal size, from photo-and-compton electrons. A similar fourfold decrease, from 16 to 4, was measured for the ^{10}B converter. The larger Cd ratio for the boron can be explained by the greater specific ionization of α's compared to electrons and consequently to the better discrimination against photo-and-compton electrons.

c) Resolution and Pressure

The modulation transfer functions were obtained in the manner described in Sec. III. The discriminator on the anode plane was set around that part of the spectrum that had the largest cadmium ratio. The results are shown in figs. 11 and 12 for each converter at 1,2,3, and 4 atm. Fig. 13 is a plot of ω_c versus pressure for each converter. There is a linear increase in resolution with pressure for both converters, but not the expected fourfold improvement. By increasing the pressure from 1 to 4 atm the improvement for boron is 110% and only a 30% improvement using Gd.

d) Resolution and Biasing

Biasing the cathodes, i.e. applying a voltage to them, modifies the electric field, particularly in the region between the lower cathode and converter. The effect of the cathode bias is to increase (with positive bias), or decrease (with negative bias) the active chamber thickness.

Fig. 14 shows the equipotential lines for the three bias cases considered. They were found using the conducting paper technique. In all cases the potential between anode and cathode remained constant. Charpak has calculated the equipotential lines for a chamber with metal strips for cathodes [2]. Far from the anode wire the equipotential lines are parallel to the cathode strips. According to this picture, there will be zero potential between the cathode and

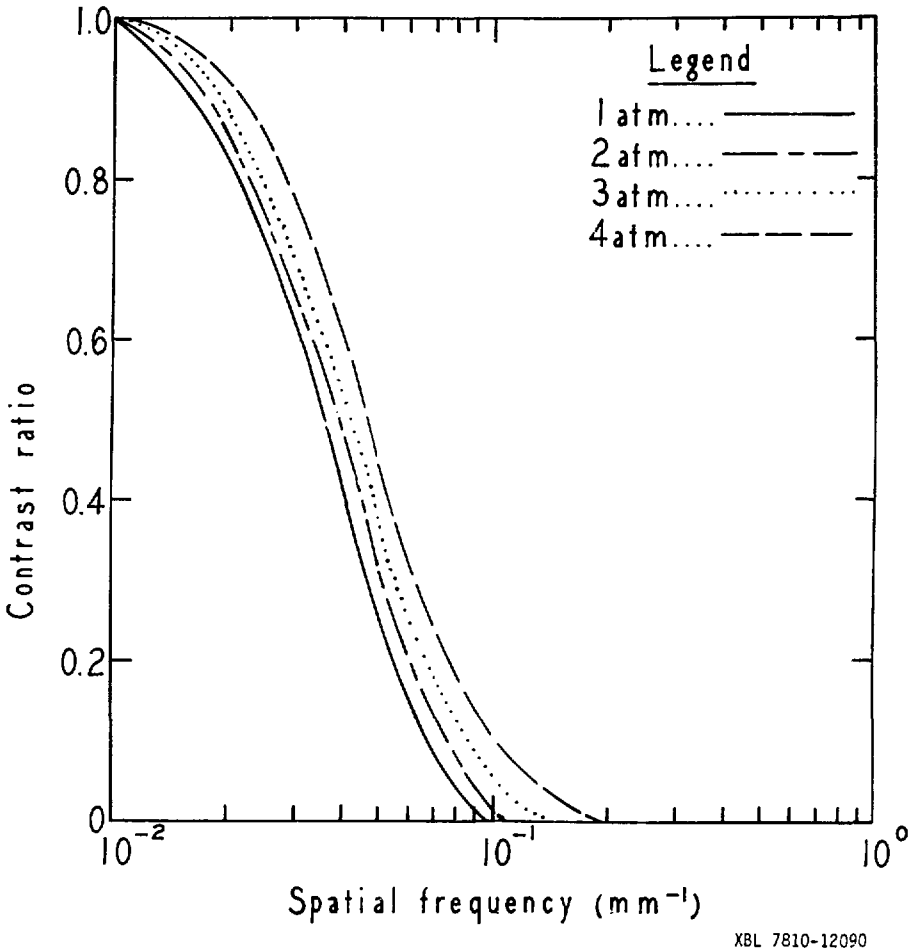

Fig. 11. MTF's using the Gd converter at 1,2,3, and 4 atm.

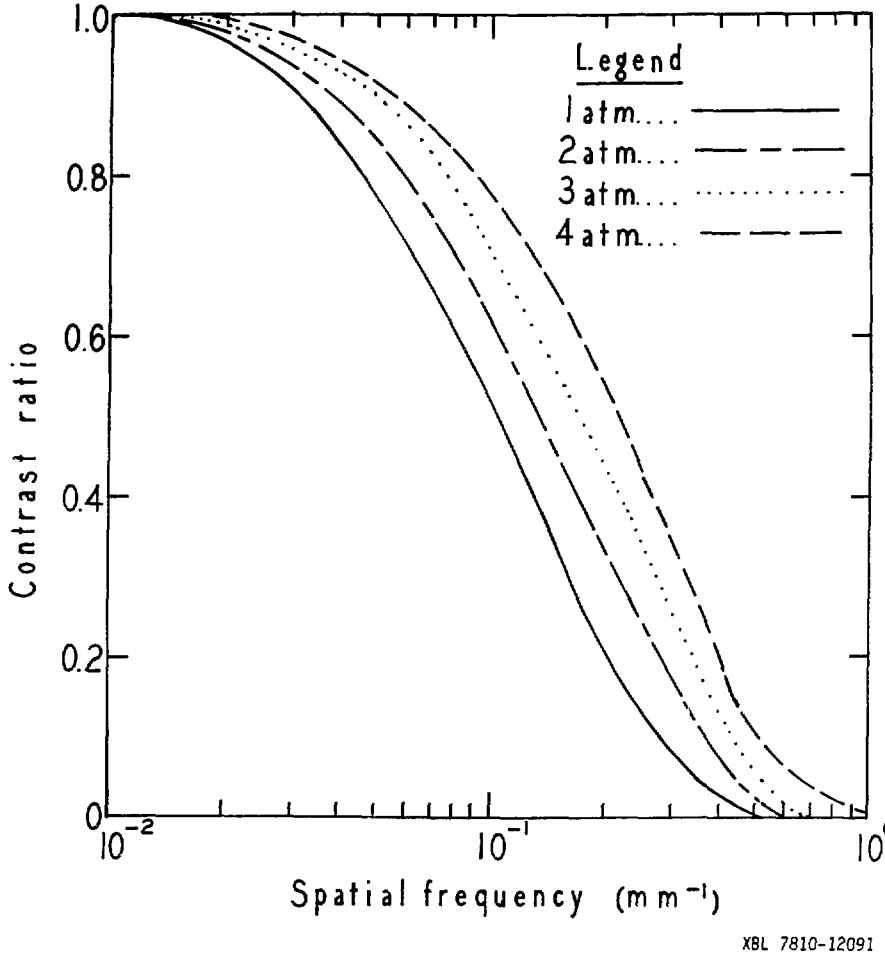

Fig. 12. MTF's using the ^{10}B converter at 1,2,3, and 4 atm.

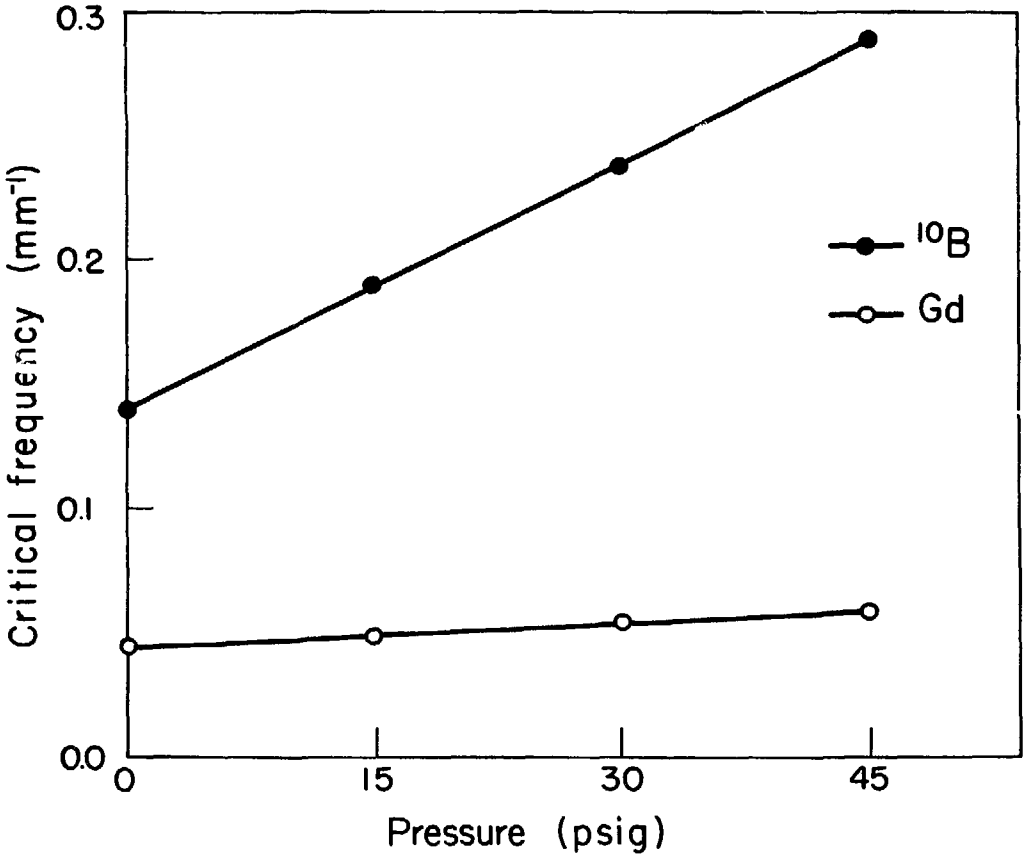

XBL 7810-6603

Fig. 13. Critical frequency, ω_c, as a function of pressure.

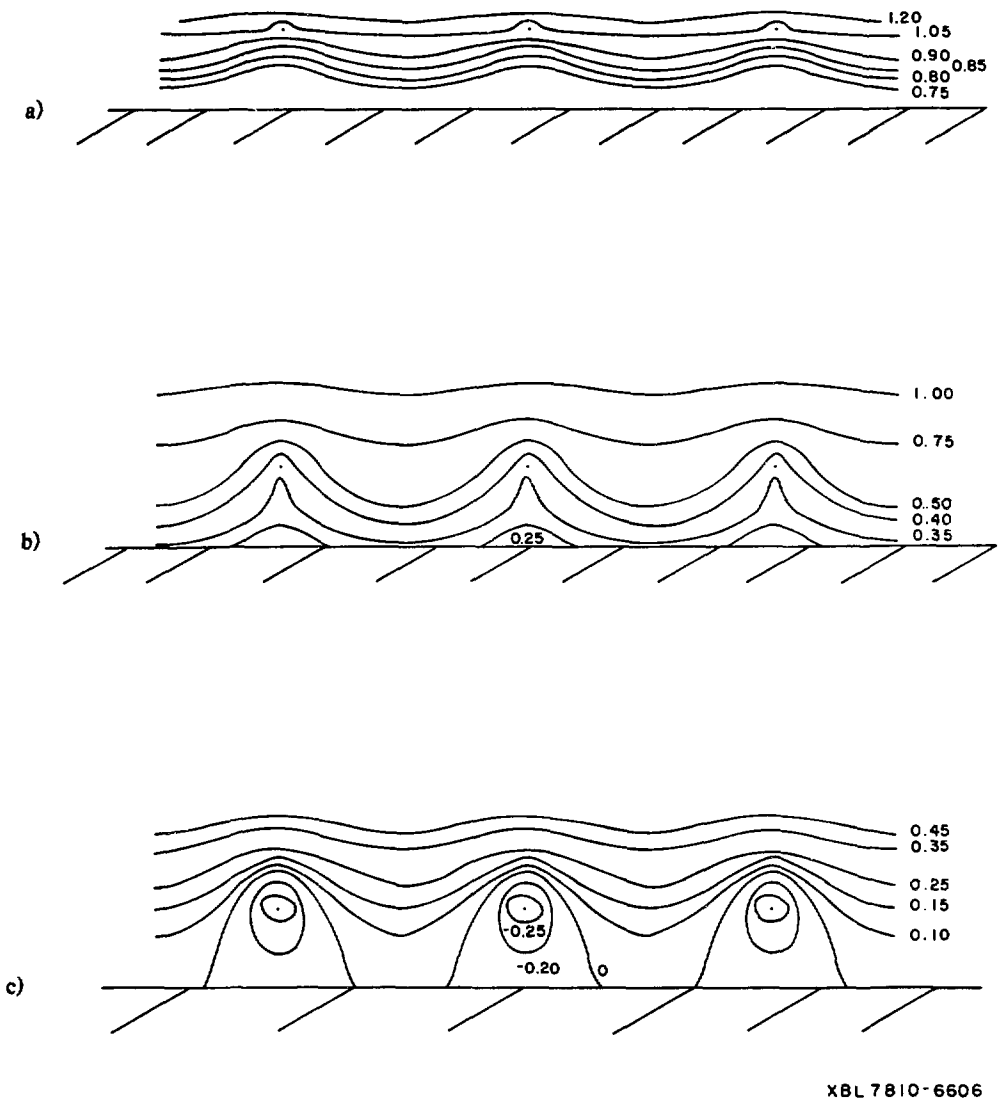

Fig. 14. Equipotential lines near and around the lower cathode and converter for a) positive bias, b) zero bias, c) negative bias. The voltages on the cathode were +1, 0, and -1 V, respectively.

converter. From fig. 14b it can be seen that there is some "leakage" of the electric field into the area below the cathode. With positive bias (fig. 14a) the leakage is increased and there is a substantial electric field near the converter, so that all particles drift toward the anode and are detected, even those that emerge far from the interaction point.

With a negative bias there are regions around each cathode wire with negative potential. Electrons with an energy less than 300 eV in these regions will drift toward the cathode and not be detected. Low energy electrons (300 eV or less) are more likely to be produced at the end of the particle's range, farthest from the point of interaction. The centroid of the ionization track will shift closer to the point of interaction than if these electrons had been included in the track, and the resolution will be improved. Those particles that are emitted at large angles and small residual energy into one of these regions, with no part of the ionization track in a region of positive potential will not be detected. This accounts for the 15% loss in efficiency that was measured whenever the bias was negative.

The ^{55}Fe source was used to explore the effects of biasing. The two cathode planes were tied together and connected to a high voltage supply. The anode voltage was changed with bias to maintain a constant anode-cathode potential. The aluminum foil that has the ^{55}Fe deposited is grounded, as is the converter. The electric field in the region between the upper cathode and the foil should be the same as the electric field around the converter and lower cathode. The countrate from the ^{55}Fe increased with positive bias and it decreased with negative bias.

The effect of biasing on resolution is shown in fig. 15 for positive and negative bias at 1 and 4 atm. with both converters. For the Gd converter there is a 10% improvement with negative bias and a 10% decrease with positive bias. With the boron converter the change is 23%, improving with -300 bias and worsening with +300.

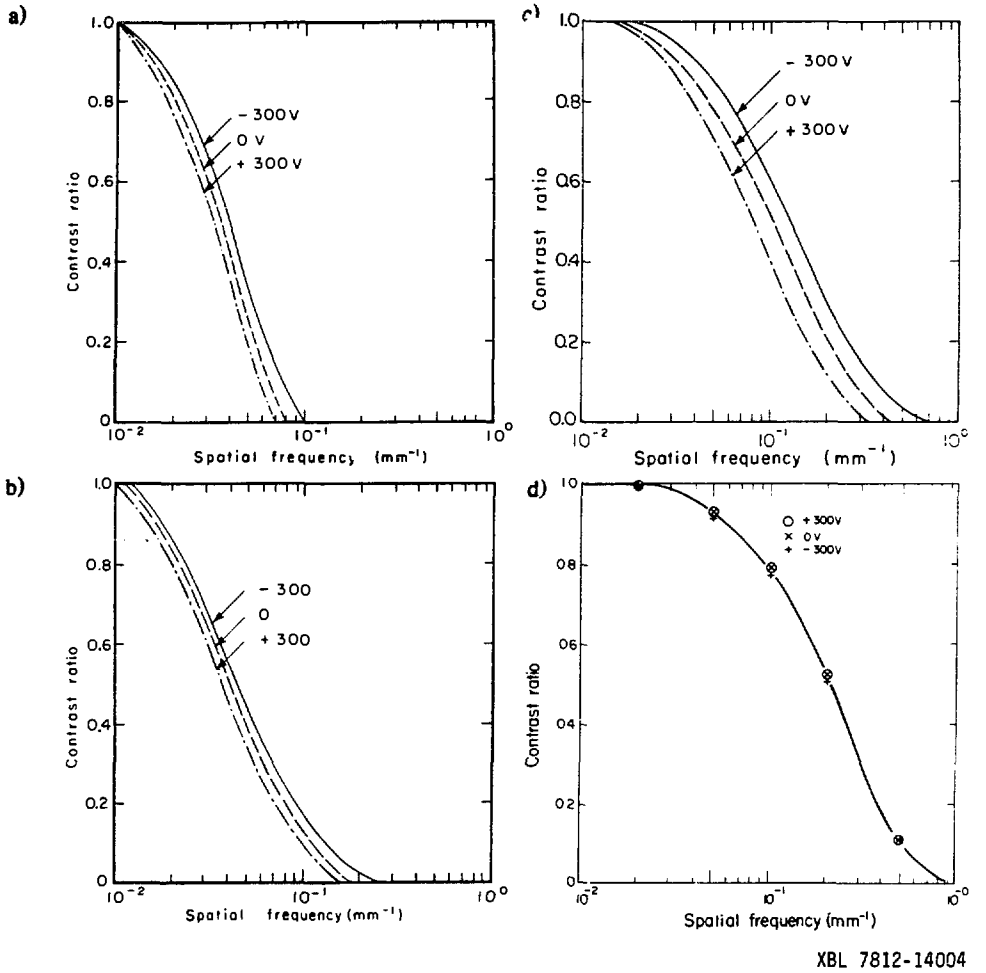

Fig. 15. MTF's taken at 0, +300, and -300 volts bias for a) Gd at 1 atm. b) Gd at 4 atm. c) ^{10}B at 1 atm. d) ^{10}B at 4 atm.

VI. Summary and Conclusions

One object of this work was to improve the spatial resolution of the wire chamber. Pressurizing the wire chamber to 4 atm increased the resolution. The amount of improvement depended on the converter, boron showing the greatest improvement. The best resolution (in terms of a single number) is 1 mm. By biasing the cathodes negatively with respect to the converter a 10 to 20% increase in resolution is obtained. Fig. 16 is a radiograph of an electric drill taken at 4 atm with the boron converter at -300 V. bias. Evidence of the improved resolution is seen in the fact that, for the first time, the strips of adhesive tape making up the boron converter show up clearly.

By increasing the pressure from 1 to 4 atm. the maximum range of the α particle was reduced to 2.5 mm. Increasing the pressure still further, and reducing the particle range should further improve the resolution. By the time the particle range is reduced to about half the wire spacing (at a pressure of 10 atm.) there shouldn't be any further improvement in resolution. The improvement of resolution with increased pressure may be limited not by the wire spacing but by the increased scattering of the incident neutrons from the thicker pressure vessel window needed at the higher pressures.

Fig. 14 shows that there are regions between cathode and converter that have positive potential. Decreasing the wire spacing by about half will make the whole area one of negative potential and there should be a further improvement in resolution using negative bias. The cost of this will be a further decrease in efficiency because all reaction products that emerge in the gas with an energy of 300 eV or less will not be detected.

Another objective was to try to improve the efficiency. As was shown in Sec. IIa the efficiency of flat converters is a function of R/λ and using the material with the smallest possible λ yields an efficiency of only 6.3%. Using pure ^{157}Gd will result in a 40% improvement in efficiency.

YSF 771-173

Appendix A

The following is a listing of the program that reads spectra from a file called mtf6 and calculates the modulation transfer function.

```
      program mtf(mtf6,output,tape9=mtf6,tape6=output)
      integer d(4,500),gback(4,500),sback(4,500)
c
c     array d=bar pattern data, gback=gamma
c     background, sback=spatial background
c
c     buff=buffer needed to read data from disk
      dimension buff(6200)
c array to hold tagwords
c
      dimension itag(4)
c
c     array for reduced data and output of
c     fast fourier transform
c
      complex a(500)
c
c     work arrays needed for fast fourier
c     transform
      dimension iwk(2000),wk(2000),ll(2000)
c
c     arrays hold starting and stopping channels for data
c     for the data
c
      dimension kstart(4),kstop(4)
c
c     for each spectra the number of bar pattern
c     cycles
      dimension ncycle(4)
c
c     work array that holds reduced data
c
      dimension xnum(500)
      data ncycle/12*1/
      data kstart/317,315,321,320/
      data kstop/461,463,456,464/
c
c     length of one bar pattern cycle in mm.
c
      xlen=20.0

c
c     read in data.  format is 4 spectra of bar
c     patterns, 4 of gamma background, and 4
c     of spatial variation
c
      do 505 l=1,4
      call lngbcd(6160,buff)
      read(9,50) itag(l),(d(l,k),k=2,500)
```

```
 50 format(2x,i4,2412x,499i6)
505 continue
    do 506 i=1,4
    call lngbcd(6160,buff)
    read(9,50) ix,(gback(i,k),k=2,500)
506 continue
    do 507 i=1,4
    call lngbcd(6160,buff)
    read(9,50) ix,(sback(i,k),k=2,500)
507 continue
c
c     ammch=the number of mm per channel
c
      ammch=0.5
      l=1
      l2=0
c
c     compute the modulation transfer function
c
      do 99 l1=1,4
      i1=l1
      l2=l2+1
      istart=kstart(l2)
      istop=kstop(l2)
      l=istart-1
      n=istop-istart+1
      q=float(n)/2.0
      n1=int(q)
c
c     compute the reduced data;subtract the gamma
c     background and divide by the spatial
c     variance. place in array a as a complex
c     number for use the the fft routine
c
      do 110 i=istart,istop
      xnum(i)=(float(d(l1,i))-float(gback(i1,i)))/float(sback(i1,i))
      a(i-l)=cmplx(xnum(i),0.0)
110 continue
      write(6,3) itag(l1)
  3 format(' ', 'the tagword is 'i5)
c
c     compute the fft
c     using the IMSL routine fftp
c
      call fftp(a,n,iwk,wk,ll)
      write(6,4)
  4 format(' ',7x,'freq.',6x,'mtf')
      do 120 j=1,n1
      freq=float(j-1)/(n*ammch)
      fact=sin(2*ncycle(l1)*freq*ammch)/((2*pi*freq*cos(freq*ammch)).
      amtf=cabs(a(j))/(cabs(a(1))*fact)
120 write(6,7) freq,amtf
  7 format(' ',2(3x,f8.4))
 99 continue
```

```
stop
end
```

The following is a listing of the calidoscope commands that will skip a number of files, in this example 16, then read the next one into a disk file called mtf6.

```
j6630.director
request,tape9,hy,x.8949
request,mtf6,pf
skpf,tape9,16,eof
copyfbf,i=tape9,o=mtf6,irl=6200,orl=6200
catalog,mtf6,rd=.
```

The following is a listing of a program that calculated the locus plot, fig. 4.

```
      program locus(input,output,tape99)
c
c     this program calculates the locus of endpoints
c     from electrons emerging from the Gd converter
c     into argon
c
      common rrange
      external resrang
c
c     the arrays x and y hold the coordinates for each
c     curve to be plotted
c     the arrays specs, bufx, bufy, are arrays used in
c     plotting
c
      dimension x(90),y(90)
      dimension specs(35),bufx(500),bufy(500)
      pi=3.1415926
c     rgd is the range in Gd (cm) of a 70 keV electron
      rgd=0.00139
c
c     initialize the specs array
c
      specs(1)=1.0
      specs(2)=1.0
      specs(3)=4.1
      specs(4)=0.0
      specs(5)=4.1
      specs(6)=0.0
      specs(7)=8.2
      specs(8)=8.2
      specs(9)=1
      specs(10)=1
      specs(11)=1
      specs(12)=99
      specs(14)=2
      specs(15)=2
      specs(16)=0
c
c     plot the grid
c
      call gdlili(specs)
c
c     from each layer in the converter, 1/25*rgd,
c     calculate the locus
      x1=float(i)*rgd/25.0
c
c     calculate the maximum angle that an electron
c     can be emitted and still reach the surface
c
      theta=acos(x1/rgd)
```

```
      itheta=int(theta*180.0/pi)
      num=0
c
c     for each 1 degree step calculate the distance the
c     electron travels in the converter until it reaches
c     the surface, its residual energy at that point,
c     and then its range in argon
c
      do 200 j=1,itheta,1
      angle=float(j)*pi/180.0
c
c     find the residual range
c
      rrange=rgd-(x1/cos(angle))
      itmax=30
c
c     use the ISML routine zfalse to find the zero of
c     the function resrang.  the result, xen, gives
c     the residual energy of the electron after
c     going a distance, rrange, in the converter.
c
      call zfalse(resrang,0.001,3,0.0001,0.071,xen,itmax,ier)
      d=range(xen,1.78,18.0)
      r=x1/cos(angle)
c
c     find the x and y coordinates of the electron
c
      x(j)=(r+d)*sin(angle)
      y(j)=(r+d)*cos(angle)-x1
      num=num+1
  200 continue
      specs(13)=num
c
c     plot the locus of points
c
      call pflili(x,y,bufx,bufy,specs)
  100 continue
      call gdsend(specs)
      stop
      end
      function resrang(energy)
c
c     this function is used to calculate the
c     residual energy of the electron in Gd
c
      common rrange
      resrang=412.0*((64.0/13.0)**0.26)*energy**(1.265-.0954*alog
     c (energy))/7900.0
      resrang=rrange-resrang
      return
      end
      function range(energy,den,z)
c
c     this function calculates the range of an electron using
```

```
c     the Katz-Penfold formula, given its energy (MeV), and
c     density (mg/cc) and atomic number of the medium
c
      range=412.0*(z**0.26)/((13.0**0.26)*den)
      range=range*energy**(1.265-0.0954*alog(energy))
      return
      end
```

Appendix B: Operating Procedure for Pressurizing the Chamber

A schematic diagram of the gas filling system is shown in Fig. A-1. The pressure transducer is a Statham strain gage type transducer. It's operating range is ± 25 psi. It was calibrated against a mercury manometer. The circuit shown in the bottom of the figure is used to zero and read the pressure transducer. The potentiometer has a resistance of 25 kΩ and the two resistors are each 10 kΩ.

Since it was necessary to measure pressures up to 45 psia, one side of the pressure transducer had to be "biased" to measure pressures greater than 25 psia.

To empty the chamber close all the valves. Turn on the vacuum pump, open valve B, then crack open valve E. When eemptying or filling the chamber valve E should not be opened more than a 1/4 to a 1/2 a turn. Changing the pressure suddenly will result in broken wires.

To zero the pressure transducer, close B and E, and open A,C,D, and F. Adjust the potentiometer until the DVM is reading zero. Close valves F and D.

To fill the pressure vessel, open valve A and open the valve on the gas regulator until the gauge is reading the desired pressure. Crack valve E and let the chamber fill until the reading on the DVM has stabilized.

If the chamber is at a higher pressure than is desired, close valve A and open E,C, and bleed the gas out through F.

To pressurize above 25 psia, pressurize the system to 25 psi. Open valve D slowly. When the DVM reads 0, close valve D. Pressurize the chamber as described above. To convert the DVM reading to pressure add the reading at 25 psi.

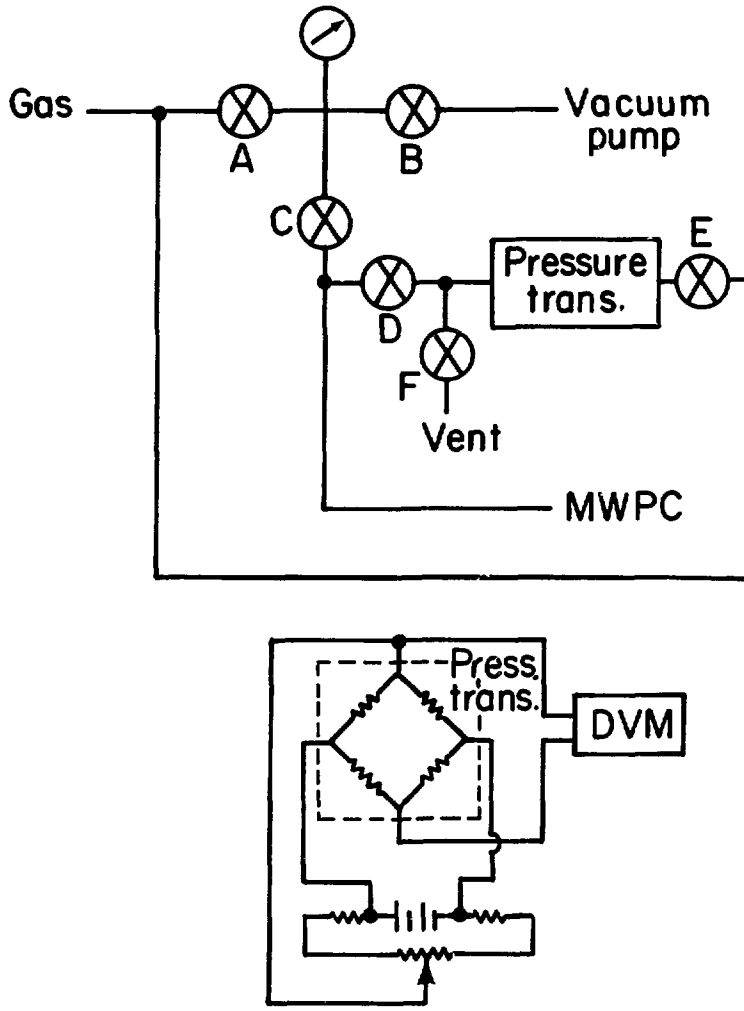

XBL 7812-14136

Fig. A-1. Schematic diagram of the chamber filling set-up and the pressure monitoring system.

References

[1] G. Charpak et al., Nuc Inst. Meth. 62 , 262 (1968)

[2] W. Frieze et al., Nuc. Inst. Meth. 136 , 93 (1976)

[3] C. Borkowski, M. Kopp, IEEE Trans. Nuc. Sci. NS-19 , 161

[4] S. Kaplan et al., Nuc. Inst. Meth. 106 , 397 (1972)

[5] G. Charpak, Ann. Rev. Nuc. Sci. 20 , 195 (1970)

[6] R. Grove et al., Nuc. Inst. Meth. 99 , 381 (1972)

[7] G. Charpak et al., Nuc. Inst. Meth. 80 , 13 (1970)

[8] K. Valentine, Development of a Multiwire Proportional Chamber for Neutron Radiography , LBL-2657

[9] R. Allemand et al., Nuc. Inst. Meth. 126 , 29 (1975)

[10] J. Alberi et al., IEEE Trans. Nuc. Sci. NS-22 , 255

[11] M. Atac, Nuc. Inst. Meth. 106 , 389 (1973)

[12] Atomic and Nuclear Data Reprints, Internal Conversion Coefficients , K. Way ed., (1973)

[13] L. Katz, A. Penfold, Rev. Mod. Phys. 24 , 28 (1951)

[14] W. Barkas, A. Rosenfeld, UCRL-8030 (1961)

[15] J. Barton, M. Klozer, Am. Soc. Nondestr. Test. Fall Conference (1970)

[16] As specified by the ASTM Subcommittee E07.05

[17] J. Barton, Journal of Materials, 7 , 18 (1972)

[18] C. Johnson, Applied Optics, 12 , 1031 (1973)

[19] P. Kowaliski, J. Photographic Science, 17 , 20 (1969)

[20] R. Baraket, S. Lerman, Applied Optics, 6 ,545 (1967)

[21] R. Ruark, W. Young, Formulas for Stress and Strain , McGraw-Hill, New York (1975)

[22] W. Diethorn, U.S. A.E.C. Report NYO-6628, as cited by M. Charles, Journal of Physics E, 5 , (1972)

Acknowledgments

It has been my pleasure to have been able to work for Prof. Selig Kaplan. I am very grateful for all the assistance and guidance he has provided.

I would also like to thank the staff of the Berkeley reactor, especially Dr. Tek Lim and Mr. Harry Braun. Thanks are also due to Mr. Jack Harrell for all his help with the electronics.

Finally, I would like to express my thanks to my parents for all their support, both moral and otherwise.

This work was supported by the U. S. Department of Energy.